

Fermi-liquid-to-polaron crossover. I. General results

A. J. Millis, R. Mueller, and Boris I. Shraiman

Bell Laboratories, Lucent Technologies, 700 Mountain Avenue, Murray Hill, New Jersey 07974

(Received 5 March 1996)

We use analytic techniques and the dynamical mean-field method to study the crossover from Fermi liquid to polaron behavior in models of electrons interacting with dispersionless classical phonons.
[S0163-1829(96)09331-9]

I. INTRODUCTION

In this paper we present results of a study of the crossover from Fermi liquid to polaron behavior in several related models of electrons interacting with dispersionless classical phonons. We use analytic techniques valid in weak and strong coupling limits, and we use the “dynamical mean-field” method¹ to obtain results at intermediate couplings. In the following paper² we present a detailed study of a more complicated model believed to be relevant to the “colossal magnetoresistance” manganites.

The electron-phonon problem has been extensively studied. The “polaron problem” of a single electron coupled to a deformable medium has been understood in detail.³ The problem of a degenerate Fermi gas coupled to phonons has been solved perturbatively in a weak coupling limit.⁴ There has also been fairly extensive work aimed at going beyond the original perturbative solution,^{5–9} but this work has been aimed mostly at understanding superconducting transition temperatures and charge-density-wave instabilities. The self-trapping or polaron physics has received less attention.

There are several experimental motivations for our work. One is the “colossal magnetoresistance” materials $\text{Re}_{1-x}\text{A}_x\text{MnO}_3$,^{10,11} where Re is a rare earth such as lanthanum and A is a divalent metal ion such as Ca or Sr. For $0.2 \leq x \leq 0.5$ these are metals at low temperatures and “insulators” (in the sense that the resistivity is high, and rises as T is lowered) at high temperatures. The insulating behavior has been argued to be due to a self-trapping of carriers in local lattice distortions.^{12,13} The physics of this material is complicated by the existence of an additional “double-exchange” carrier spin interaction, and will be discussed in the following paper.² $\text{La}_{2-x}\text{Sr}_x\text{NiO}_4$ is another compound in which carrier localization by lattice distortions has been discussed.¹⁴ Previous work on $\text{La}_{2-x}\text{Sr}_x\text{NiO}_4$ has focused on density-wave order at particular, commensurate, x but the effects discussed here are likely to be relevant also. We also mention the many semiconducting compounds that display polaron effects when very lightly doped.³ At higher dopings, electron degeneracy effects will become important, but the electron-phonon interaction will remain strong.

We study models of electrons interacting with phonons. The electrons may or may not have spin and orbital degeneracy and are coupled to one or two independent local oscillators. The motivation for studying these different but closely related models is as follows. The interplay of polaron and Fermi liquid physics is controlled by energy and entropy.

The competing energies are the electron delocalization or kinetic energy E_{kin} and the lattice energy E_{latt} gained by localizing an electron. The entropy of a localized electron depends upon the number of spin and orbital states available for it to localize into, while the entropy of the phonons depends on the phase space of the oscillators. Because the different models have different entropies, we expect them to behave differently at nonzero temperatures.

Our study has several limitations. First, the numerical results are obtained via the dynamical mean-field approximation. This is a controlled approximation, which, however, becomes exact only in a limit in which the spatial dimension $d \rightarrow \infty$.¹ Studies of other models have indicated that for $d=3$ the results are qualitatively correct and indeed in good numerical agreement with those obtained by other methods and by experiment.^{1,15} The quantitative accuracy for quasi-two-dimensional materials such as $\text{La}_{2-x}\text{Sr}_x\text{NiO}_4$ is not clear. Further, the dynamical mean-field approximation is essentially local, so intersite information (e.g., about polaron size) is difficult to obtain. We have not considered density-wave instabilities, which have been recently studied via the dynamical mean-field method.^{9,16} We have also assumed classical phonons. This approximation is known in the single-electron case not to affect the physics significantly³ (although it does lead to a few easily diagnosed low-temperature pathologies), and it dramatically simplifies the computations. However, it does mean that we are unable to study superconductivity. A third limitation is that we study models in which the only interaction is the electron-phonon interaction. In particular, we omit the on-site “Hubbard-U” Coulomb interaction, which is undoubtedly important in at least some oxide materials.^{14,17}

While the approximations we have made limit the direct applicability of some of our results to experimental data on these materials, many of our results are experimentally relevant and we believe it is useful to have a detailed account of the behavior of a well-defined model in the literature. At various places in the text we will qualitatively discuss the effects of nonclassical phonons and of the on-site Coulomb interactions, but a quantitative treatment will be left to a future publication.

The remainder of this paper is organized as follows. Section II defines the models, the parameters, and the approximations. Section III discusses the numerical methods used. Section IV presents the results of a detailed solution of the simplest model, a nondegenerate band of spinless electrons interacting with a single oscillator. We give phase diagrams,

electron spectral functions, frequency, and temperature-dependent conductivities and phonon probability distributions. Section V discusses the changes that occur if electron spin and orbital degeneracy, and multiple oscillators are included. Section VI is a conclusion. Appendix A clarifies the relation between the results presented here and those of the conventional Migdal-Eliashberg treatment of the electron-phonon problem. The other Appendices present details of various calculations.

II. MODELS AND FORMALISM

A. Hamiltonian

In this section we define the models we study and present the approximations we use. We consider electrons coupled to phonons; the Hamiltonian H may be written as the sum of an electronic part H_{el} , a phonon part H_{ph} , and an interaction part $H_{\text{el-ph}}$ as

$$H = H_{\text{el}} + H_{\text{ph}} + H_{\text{el-ph}}. \quad (1)$$

For H_{el} we take electrons moving on a lattice. An electron on a given site i may be in one of n_{orbital} orbital states (we will consider $n_{\text{orbital}}=1$ and $n_{\text{orbital}}=2$) and one of n_{spin} spin states (we will consider $n_{\text{spin}}=1$ and $n_{\text{spin}}=2$). The operator creating an electron of spin α in orbital state a on site i is $d_{ia\alpha}^\dagger$ and

$$H_{\text{el}} = - \sum_{ij} t_{ij}^{ab} d_{ia\alpha}^\dagger d_{jb\beta} - \mu \sum_{ia\alpha} d_{ia\alpha}^\dagger d_{ia\alpha}. \quad (2)$$

Here we have introduced the hopping matrix element t_{ij}^{ab} and the chemical potential μ .

We model the phonons as localized classical oscillators. We write the displacement of the oscillator from some reference position as r . We consider two cases: ‘‘one-dimensional phonons,’’ where r is a scalar quantity with $-\infty < r < \infty$, and ‘‘two-dimensional phonons’’ where \vec{r} is a two-component vector, which we parametrize by a magnitude r and an angle ϕ via $\vec{r} = r(\cos\phi, \sin\phi)$. We assume that in the absence of the electron-phonon interaction the equilibrium position of the oscillator is $r=0$, and that there is an elastic restoring force with force constant k . We measure r in units of lattice constant so r is dimensionless and k has the dimension of energy. We write

$$H_{\text{ph}} = \frac{1}{2} k r^2. \quad (3)$$

The form of the electron-phonon coupling depends on the physics. One possible coupling is of the phonon to the charge of the electron, i.e.,

$$H_{\text{el-ph}}^{\text{charge}} = g \sum_{ia\alpha} r_i (d_{ia\alpha}^\dagger d_{ia\alpha} - n). \quad (4)$$

Here we have introduced the mean density $n = (1/N) \langle \sum_{ia\alpha} d_{ia\alpha}^\dagger d_{ia\alpha} \rangle$ and have defined $r=0$ to be the equilibrium phonon state for a uniform distribution of electrons. N is the number of sites in the crystal. The electron-phonon coupling is g . If both the electrons and the phonons are degenerate, then one may have a coupling between the orbital state of the electron and the displacement of the local phonon.

Such coupling may be expected to occur in materials such as $\text{La}_{1-x}\text{A}_x\text{MnO}_3$ in which the Jahn-Teller effect is important.^{12,18,19} In such materials there are in the absence of lattice distortions two degenerate electronic states on each site, transforming as a two-dimensional representation of the cubic group. The degeneracy may be split by interaction with an appropriate phonon mode. The interaction expressing this physics is prescribed by group theory¹⁹ to be

$$H_{\text{el-ph}}^{\text{JT}} = g \sum_{iab\alpha} d_{ia\alpha}^\dagger \vec{\tau}^{ab} d_{ib\alpha} \cdot \vec{r}_i. \quad (5)$$

Here $\vec{\tau} = (\tau_z, \tau_x)$ is a vector of Pauli matrices acting in the orbital subspace and $r_z = r \cos\phi$, $r_x = r \sin\phi$.

B. Parameters and limits

One important energy scale is the electron banding or kinetic energy. This depends upon the band filling n and the details of the hopping matrix elements t_{ij}^{ab} but it is roughly of order t , where t is a typical value of t_{ij}^{ab} .

Another important energy is that obtained by localizing an electron on a site. By minimizing Eqs. (4) or (5) and (3) one finds this energy to be of order g^2/k . The ratio of these scales is the important dimensionless parameter $\lambda = g^2/kt$; $\lambda < 1$ corresponds to weak coupling and $\lambda > 1$ to strong coupling. This λ is shown in Appendix A to be related to the usual coupling constant of the Migdal-Eliashberg theory by a factor of $n_{\text{spin}} n_{\text{orb}} / \pi$.

A final important scale is the phonon frequency ω_D . In the weak electron-phonon coupling limit it is known that for $T \gtrsim \omega_D/3$, phonons behave classically while for lower T quantum effects are important.³ In the strong coupling limit, polarons are formed and large lattice distortions occur. From studies of a single electron coupled to a deformable medium³ one finds that quantum effects are important only at a very low scale ω_D/n , where $n \gg 1$ is roughly the number of quanta involved in the formation of the polaron.³ Throughout this paper we assume that T is sufficiently high that quantum effects in the phonons may be neglected.

C. Formalism

Physical quantities may be calculated from the partition function Z , which may be written as a functional integral over the electron and phonon fields. Because we have assumed classical phonons, we may solve the electron problem for given values of the phonon coordinate and then average over the phonon coordinates. Because the phonon is classical, we may rescale the phonon coordinate to $r = \sqrt{k/tr}$. The partition function becomes

$$Z = \int \mathcal{D}_{\text{phonon}} \exp \left[- \frac{1}{2} \frac{t}{T} \sum_i r_i^2 + \text{Tr} \ln [G_{\text{eff}}^{-1}] \right]. \quad (6)$$

Here T is the temperature, $\mathcal{D}_{\text{phonon}}$ is the phonon measure appropriate to the choice of phonon, and G_{eff} is the electron Green function appropriate to Eq. (1) with fixed static r_i . Note also that r has been rescaled in such a way that in $H_{\text{el-ph}}$ the coupling constant $g = \sqrt{\lambda}$.

Starting from Eq. (6) one may make perturbative diagrammatic calculations using standard methods. In the weak

coupling limit the starting point is $r_i=0$ (corresponding to uncoupled electrons and phonons) and it may be seen from the first term in the exponent of Eq. (6) that fluctuations in r are small, of order $\sqrt{T/t}$. This is the classical analogue of the Migdal expansion parameter $\sqrt{\omega_D}/t$. In the strong coupling limit the starting point has some $r_i \neq 0$ but fluctuations are still of order \sqrt{T} , so that at low- T an analytic treatment is possible, if the ground-state configuration of the r_i can be determined. The connection to the conventional treatment of the electron-phonon problem is discussed in more detail in Appendix A.

At intermediate coupling we have not succeeded in constructing the ground state about which to expand. We have therefore resorted to the ‘‘dynamical mean-field’’ approximation¹ in which it is assumed that the electron self-energy is local (i.e., momentum independent). In the electron-phonon problem in three spatial dimensions the self-energy is known to have only a weak momentum dependence in the various solvable limits,^{4,21} so the dynamical mean-field approximation, which formally becomes exact in a limit in which spatial dimensionality $d \rightarrow \infty$, seems likely to be reliable.

The electron Green function G in general depends upon orbital indices (a, b), spin indices (α, β), momentum \vec{k} , and Matsubara frequency $i\omega_n$. The dynamical mean-field ansatz is

$$G_{\alpha\beta}^{ab}(k, i\omega_n) = [i\omega_n - \Sigma_{\alpha\beta}^{ab}(i\omega_n) - \epsilon_k^{ab} + \mu]^{-1}. \quad (7)$$

Here ϵ_k^{ab} is the Fourier transform of t_{ij}^{ab} . All of the quantities in Eq. (7) are tensors in the direct product of spin and orbital space, and quantities without roman (a, b) or greek (α, β) indices are proportional to the unit matrix in orbital and spin space, respectively.

Throughout this paper we shall assume that there is no long-range order in either orbital space or spin space, so we may take $\Sigma_{\alpha\beta}^{ab} \sim \delta_{ab} \delta_{\alpha\beta}$. Generalizing the formalism to include orbital ordering would be straightforward and quite interesting. The generalization to ferromagnetic spin ordering was given by Furukawa²² and is discussed further in the following paper.² Because Σ is taken to be k independent all interaction effects are derivable from the local (k -integrated) Green function, G_{loc} . Because we have assumed that there is no long-range order in orbital space, $G_{\text{loc}}^{ab} \sim \delta_{ab}$. We may therefore write

$$G_{\text{loc}}(i\omega_n) = \frac{1}{2} \text{Tr} \int \frac{d^d k}{(2\pi)^d} G^{ab}(k, i\omega_n). \quad (8)$$

The k integral may be simplified by introducing at each k point the ab space rotation R_k , which diagonalizes G^{ab} , writing $G^{ab}(k) = R_k G_{\text{diag}} R_k^{-1}$ and exploiting the cyclic invariance of the trace. The k integrals of the two components of G_{diag} must be identical, so we may finally write

$$G_{\text{loc}}(i\omega_n) = \int \frac{d\epsilon_k \mathcal{D}(\epsilon_k)}{i\omega_n - \Sigma(i\omega_n) - \mu - \epsilon_k}, \quad (9)$$

with $\mathcal{D}(\epsilon_k)$ the density of states.

Because all interactions are local, G_{loc} may be derived from a partition function identical in form to Eq. (6) but with spatial index i suppressed and the quantity G_{eff}^{-1} replaced by

$$G_{\text{MF}}^{-1} = -a d_{\alpha\alpha}^\dagger d_{\alpha\alpha} + H_{\text{el-ph}} \quad (10)$$

at fixed phonon coordinate. The free energy corresponding to a given value of phonon coordinate may be found as usual from G_{MF} , and from this one may construct the phonon probability distribution

$$P(r) = \frac{1}{Z_{\text{loc}}} \exp \left[-\frac{r^2}{2T} + \sum_n \text{Tr} \ln G_{\text{MF}}^{-1} \right], \quad (11)$$

where the local-approximation partition function Z_{loc} is defined by

$$Z_{\text{loc}} = \int \mathcal{D}_{\text{phonon}} P(r). \quad (12)$$

Here a is a frequency-dependent effective field (analogous to the magnetization in the usual Weiss mean-field method) determined by the condition

$$G_{\text{loc}}(i\omega_n) = \frac{\partial \ln Z_{\text{loc}}}{\partial a(i\omega_n)}. \quad (13)$$

This condition may be implemented by observing that

$$\Sigma(i\omega_n) = a(i\omega_n) - G_{\text{loc}}^{-1}. \quad (14)$$

The precise form of the resulting equation depends on the density of states. We shall consider two forms, the Lorentzian,

$$\mathcal{D}_{\text{Lor}}(\epsilon_k) = \frac{t/\pi}{\epsilon_k^2 + t^2} \quad (15)$$

and the semicircular,

$$\mathcal{D}_{\text{semi}}(\epsilon_k) = \sqrt{4t^2 - \epsilon_k^2} / (2\pi t^2). \quad (16)$$

The Lorentzian density of states has the advantage that the self consistency equation may be analytically solved to yield

$$a_{\text{Lor}}(i\omega_n) = i\omega_n + \mu + it \text{sgn} \omega_n. \quad (17)$$

It has, however, two unphysical features: $\mathcal{D}_{\text{Lor}}(\epsilon_k)$ is unbounded and $\int_{-\infty}^{\infty} d\epsilon_k \epsilon_k \mathcal{D}_{\text{Lor}}(\epsilon_k) = \infty$ so the kinetic energy is infinite for finite μ .

For the semicircular density of states the ϵ_k integral may also be performed analytically, leading to

$$a_{\text{semi}}(i\omega_n) = i\omega_n + \mu - t^2 G_{\text{loc}}(i\omega_n). \quad (18)$$

This equation must be solved numerically, except in certain limits.

The semicircular density of states corresponds to a Bethe lattice and the dynamical mean-field theory together with the self-consistency condition Eq. (18) can be derived in this case by a more physically transparent argument. We take for concreteness the case of orbitally degenerate electrons with a Jahn-Teller coupling to orbitally degenerate classical phonons. On a Bethe lattice the local Green function G_{ii} on a site i with phonon amplitude r_i is

$$G_{ii}^{ab-1}(i\omega_n, r_i) = i\omega_n + \mu + g\vec{r} \cdot \vec{\tau}^{ab} - \sum_{jcd} t_{ij}^{ac} G_{jj}^{cd}(i\omega_n, r_j) t_{ji}^{db}. \quad (19)$$

One may diagonalize the Jahn-Teller coupling by a local rotation R_i in orbital space, with $R_i = \cos\phi_i/2\tau_z + \sin\phi_i/2\tau_x$, and one may absorb R_i into the hopping matrix $\hat{t}_{ij} = R_i t_{ij} R_j$, which thus acquires a dependence on the relative orientation of the phonon distortions. The mean-field theory for the disordered phonon state follows (in the limit of large coordination number Z_{coord}) from the assumptions that the ϕ_j 's and r_j are statistically independent and the hopping t_{ij} scales as $t/\sqrt{Z_{\text{coord}}}$. The sum on j can then be replaced by an average over ϕ 's and r 's, the latter with a nontrivial distribution $P(r)$ defined by Eq. (11). The hopping self-energy then reduces to $\delta^{ab} G_{\text{loc}}$ with $G_{\text{loc}} = 1/2\text{Tr}\langle G_{ii} \rangle_{r_i}$ and the self-consistent equation for G_{loc} is obtained by averaging G_{ii} given by Eq. (19) over r_i . Equation (19) may be helpful as a starting point for mean-field theories with nontrivial spatial correlations of the phonons.

We will be interested in three physical quantities: the momentum-integrated electron spectral function $A(\omega)$, the phonon probability distribution $P(r)$, and the conductivity σ . The spectral function is

$$A(\omega) = -\frac{\text{Im}G_{\text{loc}}(i\omega_n \rightarrow \omega + i\epsilon)}{\pi}. \quad (20)$$

In the dynamical mean-field method the conductivity $\sigma_{ab} = \sigma_{\text{MF}} \delta_{ab}$ (here a, b are coordinates axes x, y, z) with

$$\sigma_{\text{MF}}(i\Omega) = \frac{e^2 t^2}{i\Omega} \text{Tr} \int d\epsilon_p \mathcal{D}(\epsilon_p) T \times \sum_{i\omega} \mathbf{G}(p, i\omega) \mathbf{G}(p, i\omega + i\Omega). \quad (21)$$

In particular, the dc conductivity is

$$\sigma_{\text{dc}}(T) = e^2 t^2 \text{Tr} \int \frac{d\epsilon d\omega}{\pi} \mathcal{D}(\epsilon_p) \times [\text{Im}\mathbf{G}(\epsilon_p, \omega)]^2 / 4T \cosh(\omega/2T)^2, \quad (22)$$

with $\mathbf{G}(\epsilon_p, \omega)^{-1} = \omega + \mu - (\epsilon_p^{ab}) - \Sigma(\omega)$.

As $T \rightarrow 0$, two possibilities arise: either $\Sigma''(\omega=0) \rightarrow 0$ or it tends to a finite nonzero value. In the former case,

$$\sigma_{\text{dc}} \rightarrow e^2 t^2 n_{\text{spin}} n_{\text{orb}} \mathcal{D}(\epsilon^*) \int \frac{d\omega}{4T} \frac{1}{(\cosh^2 \omega/2T)} \frac{1}{\Sigma''(\omega, T)}, \quad (23)$$

with ϵ^* satisfying $\epsilon^* = \mu - \Sigma'(0)$. In the latter case

$$\sigma_{\text{dc}} \rightarrow \frac{e^2 t^2}{\pi} n_{\text{spin}} n_{\text{orb}} \int d\epsilon_p \mathcal{D}(\epsilon_p) \times \left[\frac{\Sigma''(0)}{[\epsilon_p + \mu - \Sigma'(0)]^2 + \Sigma''(0)^2} \right]^2. \quad (24)$$

III. NUMERICAL METHODS

In this section we outline the numerical methods used to solve Eq. (18) and compute physical quantities. To aid in the discussion we write this equation explicitly for the simplest case of nondegenerate electrons coupled to nondegenerate phonons. We have, setting $t=1$,

$$a(\omega) = i\omega + \mu - \int_{-\infty}^{\infty} dr \frac{P(r)}{a(\omega) + gr}, \quad (25)$$

with

$$P(r) = \frac{1}{Z_{\text{loc}}} \exp \left[-\frac{r^2}{2T} + \sum_n \ln \left(\frac{a_n + gr}{i\omega_n} \right) \right] \quad (26)$$

and Z_{loc} given by Eq. (12). Here $a_n = a(i\omega_n)$ with ω_n a fermion Matsubara frequency $\omega_n = (2n+1)\pi T$.

For most physical quantities we require $a(\omega)$ for real frequency. It is possible to express $P(r)$ in terms of $a(\omega)$, but this involves performing numerically an integral over a continuous frequency. We have found it more convenient to find $P(r)$ by solving Eq. (25) on the Matsubara points and then using this $P(r)$ to solve for $a(\omega)$ on the real axis. In what follows we first discuss the solution on the Matsubara axis and then mention the additional issues arising for the real axis case.

We solve Eq. (25) on the Matsubara axis by direct iteration, so that a_n at step $N+1$ is determined by evaluating the right-hand side of Eq. (25) using a_n from step N . If a solution at the same coupling and a nearby temperature is available we use this as the starting point; if not we use the $g=0$ solution. Convergence is usually rapid; typically 10 iterations are required for convergence from the $g=0$ solution to a solution with rms error of 10^{-5} (averaged over all retained Matsubara frequencies) and using the solution from a nearby T saves about 2 iterations. However, away from half filling, in the strong coupling limit, the straightforward iteration procedure does not converge, but instead goes to a two-step limit cycle in which evaluating the right-hand side of Eq. (25) using the values $a_n^{(1)}$ yields a different set of values $a_n^{(2)}$ which, when put back in Eq. (25), generate again $a_n^{(1)}$. This limit cycle may be avoided by making the iteration proceed in smaller steps by defining a_n at step $N+1$ to be an appropriate linear combination of the right-hand side of Eq. (25) and the solution at step N ; however, as T gets lower or coupling gets stronger the required admixture of the newly computed a gets smaller, and at some point the computations become too time consuming.

Away from half filling it is necessary at each temperature and coupling to find the chemical potential $\mu(T, g)$, which gives the desired n . We do this by computing at several values of μ and interpolating. At strong coupling and low- T , n is a very sensitive function of μ , and it is necessary to choose at least three μ values all of which yield n 's, which are within 10 % of the desired value and to use a cubic interpolation. In the calculations presented n varies by less than 6×10^{-4} over the range of T and g considered. We found it convenient to evaluate n via

$$n = \lim_{\tau \rightarrow 0} T \sum_n \text{Tr} G_{\text{loc}}(i\omega_n) e^{-i\omega_n \tau}. \quad (27)$$

G_{loc} may be expressed in terms of a_n via the mean-field equations.

The next issue is the number of Matsubara points needed to compute $P(r)$ accurately. We note from Eq. (25) that at large ω_n

$$a_n = i\omega_n + \mu - \frac{1}{i\omega_n} - \frac{1}{\omega_n^2} \int dr P(r) (\mu + gr) + O\left(\frac{1}{\omega_n^3}\right). \quad (28)$$

Analogous but slightly different formulas apply in the case of Jahn-Teller coupling. We determine the maximum retained Matsubara frequency n_{max} by requiring that the $O(1/\omega_n^3)$ terms are less than 10^{-5} and in the expression for $P(r)$ we evaluate the terms with $|n| > n_{\text{max}}$ analytically, using the a_n given in Eq. (28); the errors are of order n_{max}^{-2} . Equation (28) is also useful for improving the accuracy of the computation of the density n from Eq. (27) away from half filling. To achieve the stated accuracy we found it necessary to choose n_{max} so that $\omega_{n_{\text{max}}} = 2\pi T(n_{\text{max}} + 1/2)$ is about 5 times the full width of the real-axis electron spectral function. The $1/T$ growth of n_{max} as $T \rightarrow 0$ limits our ability to calculate at very low-temperatures. For example, at $g = 1.29$ and $T = 0.02$, $n_{\text{max}} \approx 250$.

The remaining numerical issue for the Matsubara-axis solution is the integral over the phonon coordinate, which is done using the numerical quadrature routine ‘‘quad’’ from the ‘‘Port’’ library. Gaussian quadrature routines are faster at weak coupling, but fail at strong coupling and low- T where $P(r)$ has a large narrow peak at an *a priori* unknown location far from the origin.

We now turn to the real axis calculations, which we also do by direct iteration of Eq. (25) with analytically continued frequency $\omega + i\epsilon$, using $P(r)$, which has already been computed. The limit cycles that plagued the Matsubara calculations do not occur, but other numerical problems arise. Because $P(r)$ is held fixed, different frequencies decouple and the mean-field equation does not come from minimizing a free energy. Nearby frequencies are also sometimes found to converge at different rates. In parameter regimes in which the $T=0$ spectral function has a gap, the imaginary $a''(\omega)$ part of $a(\omega)$ is small and very temperature-dependent at low T for frequencies in the gap. Our procedure fails to find a nonzero value of a'' if this quantity becomes less than 10^{-3} , and we are not sure of the accuracy for $a'' \leq 10^{-2}$. Physical properties in such regimes depend crucially on the tailing of the spectral function into the gap, so our ability to calculate the low T properties of regimes with gaps is limited.

To calculate conductivities we solve the real axis mean-field equations for a discrete set of frequencies spaced by 0.01. Then at these frequencies we evaluate

$$\theta(\omega) = \int d\epsilon_p \mathcal{D}(\epsilon_p) [\text{Im}G(\epsilon_p, \omega)]^2 \quad (29)$$

using the Port routine ‘‘quad’’ and then obtain

$$\sigma \approx n_{\text{spin}} n_{\text{orb}} \int d\omega \theta(\omega) \cosh^{-2} \frac{\omega}{2T} \quad (30)$$

using the quad routine and evaluating $\theta(\omega)$ by spline interpolation from the known values. In the computation we set the factors $e^2/\pi = 1$.

We note finally that especially in the crossover region where there is a frozen-in lattice distortion that is not large enough to open a gap in the spectral function, physical properties are quite sensitive to the precise value of the coupling constant. A change in g by 2% can lead to more than factor of three changes in, e.g., the low- T conductivity; also small numerical errors in the computation of the Fermion contribution to the action can mimic a small change in g . An example can be found in the curve labeled $g = 1.60$ in Fig. 2. The analytically calculated $T=0$ resistivity for this g is 3.75. The actual numerically calculated low- T spectral function is found to be essentially identical to that calculated analytically at $T=0$ for $g = 1.57$; the corresponding analytical $T=0$ resistivity is found to be 1.004, in good agreement with the numerical calculation.

IV. NONDEGENERATE SPINLESS ELECTRONS

A. Introduction

In this section we present results of a detailed study of a model of spinless, orbitally nondegenerate Fermions coupled to classical nondegenerate oscillators. This section is organized as follows. In this section, we outline the qualitative physics. In Sec. IV B we solve the original model, Eqs. (1)–(4) in simple limits, obtaining results that clarify the interpretation of the $d=\infty$ results. In Sec. IV D we solve the $d=\infty$ model with the Lorentzian density of states [Eqs. (12) and (17)], and in Sec. IV D the $d=\infty$ model with semicircular density of states [Eqs. (12) and (18)].

In the model defined by Eqs. (1)–(4) we may distinguish three phases according to the $T \rightarrow 0$ limits of the oscillator coordinate r and the electron spectral function. In *weak coupling*, $\lim_{T \rightarrow 0} \langle r \rangle = 0$ and the spectral function takes the noninteracting form. The low- T resistivity is then linear in T , and extrapolates to 0 as $T \rightarrow 0$, being due to the thermal fluctuations of r about $r=0$. In *intermediate coupling*, $\lim_{T \rightarrow 0} \langle r \rangle \neq 0$, implying that some frozen-in lattice distortions exist. However, the amplitude of these distortions is too small to localize states near the Fermi level. The low- T resistivity is still linear in T , but extrapolates to a nonzero value at $T=0$. The spectral function is perturbed from its noninteracting form. In *strong coupling* the amplitude of the frozen-in lattice distortions is large enough to localize electrons at the Fermi level, leading to a gap in the $T=0$ spectral function and an activated resistivity.

All three regimes are found in the calculations discussed below. None of the regimes involves long-range order—the localization should be thought of as being due to polaron formation. At commensurate filling or in low dimensions, effects of long-range order (i.e., charge-density-wave formation or polaron ordering) will be important but at general incommensurate fillings these effects will be important only at low T and for our purposes may be neglected. Further discussion may be found, e.g., in Refs. 9 and 16.

Quantum effects will also be important: at sufficiently low T and in the absence of long-range order, quantum tunneling will restore translational invariance. In the strong coupling limit the quantum effects may be thought of as leading to the formation of a polaron band, with a bandwidth exponentially small in λ ; at scales greater than the polaron bandwidth the results presented here will apply. The effect of quantum fluctuations on the intermediate coupling regime is less clear, but must be left for future work.

B. Full model, solvable limits

The crucial issue is performing the integral over the phonon coordinates in Eq. (6). At low T the integral is sharply peaked about particular values $\{r_i^*\}$ and a steepest-descent approximation is possible. Two solvable cases occur:

(1) *Weak coupling.* For $\lambda < \lambda_c$ and $T \rightarrow 0$ (λ_c will be estimated below) $r_i^* \equiv 0$ and one may expand the logarithm in Eq. (6) obtaining

$$Z \propto \exp[\text{Tr} \ln G_0^{-1}] \int \mathcal{D}r_k \exp\left[-\frac{t[1 - \lambda B(k)]r_k r_{-k}}{2T}\right]. \quad (31)$$

Here $G_0^{-1} = i\omega_n - \epsilon_k + \mu$ and

$$B(k) = t \int \frac{d^3p}{(2\pi)^3} \frac{f(\epsilon_{p+k}) - f(\epsilon_p)}{\epsilon_p - \epsilon_{p+k}}. \quad (32)$$

It is evident from Eq. (31) that the expansion in powers of r about $r_i \equiv 0$ is controlled at low- T if $\lambda < \lambda_c$ with

$$\lambda_c^{-1} = \max_k B(k). \quad (33)$$

In particular, as $T \rightarrow 0$ at fixed λ , $r_k \sim \sqrt{T}$ is small, so the leading-order perturbation expression for the Fermion self-energy Σ applies.^{4,21} This expression is

$$\Sigma(p, i\omega, T) = \lambda T \int \frac{d^3k}{(2\pi)^3} \frac{1}{1 - \lambda B(k)} \frac{t}{i\omega - \epsilon_{p+k}}. \quad (34)$$

For small ω , we may restrict the k integral to wave vectors such that $p' = p + k$ is on the Fermi surface. The leading contribution to the ω dependence of Σ is then

$$\begin{aligned} \Sigma(p, i\omega, T) &= i\pi T \lambda \text{sign}(i\omega) \\ &\times \int \frac{d\Omega_p'}{4\pi} \mathcal{D}(\epsilon_{p'}) / [1 - \lambda B(p - p')] \end{aligned} \quad (35)$$

and if also $\lambda \ll \lambda_c$

$$\Sigma(p, i\omega, T) = i\pi T \lambda \bar{\mathcal{D}}(\epsilon_F) \text{sgn}\omega \quad (36)$$

with $\bar{\mathcal{D}}(\epsilon_F)$ the angle averaged density of states at the Fermi surface.

Equation (36) is shown in Appendix A to be precisely the usual Migdal expression for the self-energy. If $(\lambda_c - \lambda)/\lambda_c$ is not too small, the quantity $\lambda T \int (d\Omega_{p'}/4\pi) \mathcal{D}(\epsilon_{p'}) / [1 - \lambda B(p - p')]$ depends only weakly on p ; if it is averaged over p on the Fermi surface it becomes the classical limit of the usual “ $\alpha^2 F$ ” function. Here T/t plays the role of the usual Migdal parameter ω_D/E_F . As $\lambda \rightarrow \lambda_c$, the phonon propagator becomes large and also acquires a singular momentum dependence because the phonon propagator

diverges at a particular wave vector, so one may expect the Migdal approximation to fail. A discussion of corrections to the Migdal approximation is beyond the scope of this paper. Note also that $\lambda < \lambda_c$ is the condition for the linear stability of the $r_i \equiv 0$ state. A $T=0$ first-order transition at $\lambda^* < \lambda_c$ to a state with $r_i \neq 0$ is possible and indeed will be demonstrated using the dynamical mean-field approximation.

The resistivity may also be computed. If $\lambda \approx \lambda_c$, the momentum dependence of the phonons may be important and vertex corrections must be considered. If $\lambda \ll \lambda_c$ the momentum dependence of the phonons, and therefore the vertex corrections, may be neglected and the conductivity on the Matsubara axis is

$$\begin{aligned} \sigma_{ab}(i\Omega_n) &= \frac{e^2}{i\Omega_n} \int \frac{d^3p}{(2\pi)^3} T \sum_{i\omega_n} \frac{\partial \epsilon_p}{\partial p_a} \frac{\partial \epsilon_p}{\partial p_b} \\ &\times G(p, i\omega_n + i\Omega_n) G(p, i\omega_n). \end{aligned} \quad (37)$$

Substituting Eq. (35) into Eq. (37), performing the integrals, and analytically continuing gives

$$\sigma(T) = \frac{e^2}{2\pi\lambda T} \int \frac{d\Omega_p}{4\pi} (v_F^a)^2 \mathcal{D}(\Omega_p). \quad (38)$$

In a simple tight binding model, $v_x(p) = 2t \sin p_x$ and evaluating Eq. (38) yields

$$\rho(T) = \frac{\pi\lambda T}{t^2 e^2 \bar{\mathcal{D}}(\epsilon_F)}. \quad (39)$$

(2) *Full model, strong coupling.* In the limit $\lambda \gg \lambda_c$ an analytic solution is possible because we may treat the electron kinetic energy as a perturbation. If it is neglected then to solve Eqs. (1)–(4) we note that if the mean density is n and the number of lattice sites is N then there are nN sites with one electron, and $(1-n)N$ sites with no electron. On the nN occupied sites there is a lattice distortion of amplitude

$$r_{\text{occ}}^* = -(g/k)(1-n) \quad (40)$$

and on the $(1-n)N$ unoccupied sites

$$r_{\text{unocc}}^* = (g/k)n. \quad (41)$$

The energy density gained may be found from Eqs (1)–(4) by neglecting the electron hopping term and evaluating the on-site energy of occupied and unoccupied sites. The result is

$$E_{\text{gained}} = -\frac{1}{2}t\lambda n(1-n). \quad (42)$$

Perturbative corrections (in powers of the kinetic energy) may be calculated.⁹ These involve processes in which electrons make virtual hops to unoccupied neighboring sites, and lead to a repulsive short-ranged interaction of order t/λ between polarons. This interaction will lead to polaron ordering, at a scale generically much lower than t/λ . In this limit transport is thermally activated; the prefactor is t and the gap is E_{gained} .

C. Dynamical mean field method: Lorentzian density of states

In this section we discuss the solution of the dynamical mean-field equations for spinless Fermions with Lorentzian density of states coupled to a single scalar oscillator. We begin with the $T \rightarrow 0$ limit, where one may use a steepest-descent approximation. The details are given in Appendix B. We find that for $\lambda < \lambda_c(n)$, $r^* = \lim_{T \rightarrow 0} \langle r \rangle = 0$, while for $\lambda > \lambda_c$ there are two extrema, at $r_1^* < 0$ and $r_2^* > 0$. For $n = 1/2$, $r_1^* = -r_2^*$, the transition at λ_c is second order: the second derivative of the energy $E(\lambda)$ has a discontinuity and r^* grows smoothly with λ . For $n \neq 1/2$, $r_1^* \neq -r_2^*$ and the transition is first order: the first derivative of $E(\lambda)$ has a discontinuity and r^* jumps discontinuously.

The physical content of the $r^* \neq 0$ states is most clearly seen from the electron Green function, which at $T = 0$ is

$$G_{\text{loc}}(i\omega) = \frac{Z_1}{i\omega + \mu + it \operatorname{sgn}\omega + gr_1^*} + \frac{Z_2}{i\omega + \mu + it \operatorname{sgn}\omega + gr_2^*} \quad (43)$$

with $Z_1 = |r_2^*| / (|r_1^*| + |r_2^*|)$ and $Z_2 = |r_1^*| / (|r_1^*| + |r_2^*|)$. Thus if $r^* \neq 0$ the spectral function consists of two resonances. In the large λ limit, these are well separated. One, of weight n , is at the negative energy $\mu - g(1 - n)$ and corresponds to the sites on which the electron-phonon interaction has localized an electron. The other, of weight $1 - n$, is at the positive energy $\mu + gn$ and corresponds to the empty sites. The splitting, $\Delta E \propto \lambda$ as expected, while the energy gained E_{gained} (relative to the undistorted state) is

$$E_{\text{gained}} = -\frac{1}{2} \lambda t n (1 - n), \quad (44)$$

consistent with Eq. (42). The Lorentzian density of states is pathological in that, as may be seen from Eq. (43), at any value of g the $T = 0$ spectral function is nonzero at $\omega = \mu$; thus the ground state is always metallic. This pathology may be traced back to the nonintegrability of the first moment of density of states, which implies that some carriers have arbitrarily large velocities and cannot be localized by any lattice distortion.

D. Dynamical mean-field method: Semicircular density of states

In this section we present results obtained using the dynamical mean-field method with semicircular density of states. Our analysis is based on Eqs. (12) and (18). The technical differences from the previously discussed Lorentzian case are that the mean-field function $a(\omega)$ satisfies a non-trivial self-consistency equation, and the moments of the density of states are finite, so the spectral function may develop a gap.

As in Sec. IV C, one may use steepest-descent arguments for T near zero. The details of the analysis are given in Appendix C. For $g < g^*$ the energy minimum is at $r^* = 0$; for $g > g^*$ there are two minima, at $r = r_1 > 0$ and $r = r_2 < 0$. For $n = 1/2$ the transition is second order and occurs at $g^* = g_c^* = \sqrt{3} \pi / 2 \cong 1.535$; for $n \neq 1/2$ the transition is first-order and occurs at a $g^* > g_c$.

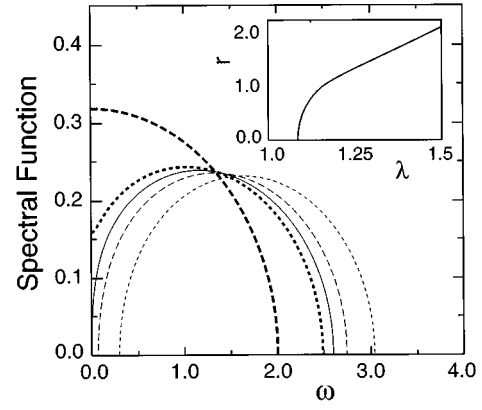


FIG. 1. Momentum-integrated electron spectral function $A(\omega)$ plotted against frequency ω for nondegenerate electrons coupled to nondegenerate phonons at density $n = 1/2$, temperature $T = 0$, and several different values of frozen-in lattice distortions $r = 0$ (heavy dashed line), 0.87 (heavy dotted line), 1.0 (light solid line), 1.17 (light dashed line) and 1.49 (light dotted line) corresponding to $g = 1.53, 1.60, 1.63, 1.69, \text{ and } 1.83$, respectively. Inset: coupling constant (λ) dependence of r .

As in Sec. IV C, the physical content of the $r^* \neq 0$ solutions is the existence of frozen-in lattice distortions. The effect of these may be seen from the local Green function, which, at $T = 0$, is

$$G_{\text{loc}} = \left(\frac{Z_1}{a(\omega) + gr_1} + \frac{Z_2}{a(\omega) + gr_2} \right) / (Z_1 + Z_2). \quad (45)$$

Here $Z_1 > 0$ and $Z_2 > 0$ are the relative weights of the free energy minima corresponding to $r = r_1$ and $r = r_2$, respectively.

Figure 1 shows $A(\omega) = -\text{Im}G_{\text{loc}}$ for $n = 1/2$, $T = 0$, and different values of $r_1 = r_2 = r$. Our interpretation of these results is that for $0 < r < 1/2$ the potential fluctuations due to the frozen-in phonons are very weak, and merely localize a few states at the band tails. This accounts for the slight broadening of A and the slight decrease near $\omega = -\mu$. For $1 > r > 1/2$ the potential is strong enough to create a minimum in A at $\omega = -\mu$; for $r > 1$ it is strong enough to localize all of the electrons and create a gap in the spectral function. Note also that as shown in the inset to Fig. 1, r is a rapid function of λ in the region $r < 1$. This rapid growth of r means that the transition is very nearly first order even for $n = 1/2$. Figure 2 shows the temperature-dependence of the resistivity for the same coupling constants used to construct Fig. 1. The two lowest resistivities are calculated for weak couplings $g < g_c$ and $g = g_c$, for which $\lim_{T \rightarrow 0} r^*(T) = 0$ (so the $T = 0$ spectral functions are identical). For $g < g_c$, $\rho(T)$ at low T is linear in T with a g dependent prefactor and $\lim_{T \rightarrow 0} \rho(T) = 0$. For $g = g_c$ the quadratic term in the phonon energy vanishes and $\rho \sim T^{1/2}$ at low- T . For g slightly greater than g_c , $\lim_{T \rightarrow 0} \rho(T) \neq 0$ but is finite. For g large enough that the spectral function has a minimum at $\omega = 0$, the resistivity initially drops as T is increased from $T = 0$. For g large enough that the $T = 0$ spectral function has a gap, ρ rises rapidly, and ultimately exponentially as $T \rightarrow 0$. The temperature at which ρ begins to rise rapidly is somewhat less than

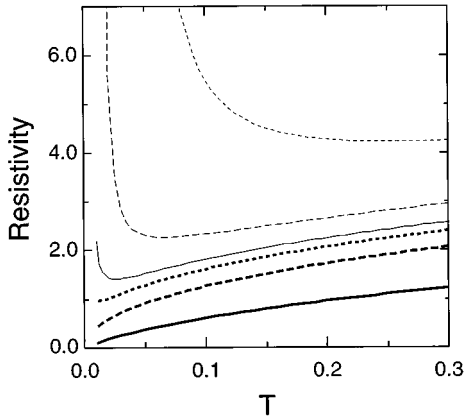


FIG. 2. Temperature (T) dependence of resistivity ρ calculated for nondegenerate electrons coupled to nondegenerate phonons at density $n=1/2$ for the coupling constants used to create Fig. 1: $g=1.29$ (heavy solid line), 1.53 (heavy dashed line), 1.60 (heavy dotted line), 1.63 (light solid line), 1.69 (light dashed line), and 1.83 (light dotted line). Note that $g=1.29$ and 1.53 have the same lattice distortion $r=0$ at $T=0$ and therefore the same spectral function.

the $T=0$ gap. Note that for $\sqrt{3\pi}/2 < g < 1.63$ $\lim_{T \rightarrow 0} \rho(T) = \rho(0)$ is neither zero nor infinite.

Some insight into the process of gap formation can be gained from Figs. 3 and 4, which show the temperature evolution of the spectral function and phonon probability distribution for coupling $g=1.69$. One sees from Fig. 2 that the rise in resistivity as T is decreased begins at $T=0.07$ at which, one sees from Fig. 3, the spectral function first develops a minimum. A weak maximum in $P(x)$ is visible in Fig. 4 even at higher-temperatures, but the maximum becomes an obvious feature at the temperature at which the resistivity begins to turn up. The initial rapid rise in the resistivity is associated with the development of the minimum in the spectral function; the asymptotic low- T behavior $\rho \sim e^{\Delta/T}$ occurs

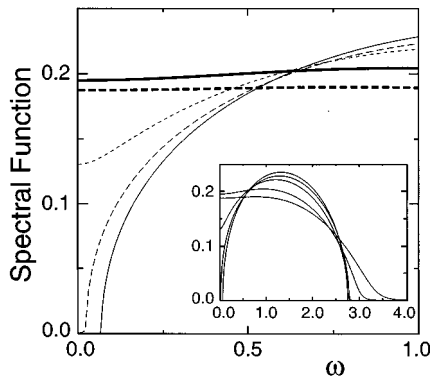


FIG. 3. Temperature (T) dependence of electron spectral function $A(\omega)$ for $g=1.69$, $n=1/2$, and $T=0$ (light solid line), 0.01 (light dashed line), 0.02 (light dotted line), 0.07 (heavy solid) and 0.15 (heavy dashed line). Inset: spectral function plotted over a wider range of frequency for parameters used in main figure. The higher the T the longer the high frequency tail. Comparison to the appropriate curve in Fig. 2 shows that the rise in the resistivity begins at the $T=0.07$ at which A first begins to develop a minimum at $\omega=0$.

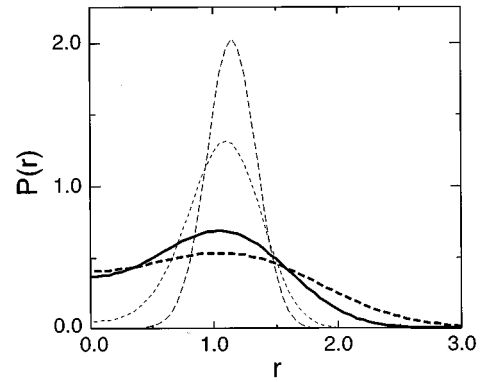


FIG. 4. Temperature-dependence of phonon probability distribution $P(r)$ for $g=1.69$, $n=1/2$, and $T=0.01$ (light dashed line), 0.02 (light dotted line), 0.07 (heavy solid line), and 0.15 (heavy dashed line).

at or below the lowest-temperatures available numerically. The numerical calculations in this section have all been performed at $n=1/2$, where particle-hole symmetry implies $\mu=0$, simplifying the computation. Results for the particle-hole asymmetric case in other models will be presented below. In our computations to date we have found that $n \neq 1/2$ has qualitatively similar behavior to $n=1/2$ with metallic and insulating regimes according to whether or not the $T=0$ spectral function has a gap. As shown by the explicit calculations of Appendix C, somewhat stronger couplings are required to obtain insulating behavior at $n \neq 1$ than at $n=1$. In the numerical calculations at $T>0$, we have seen no evidence of the first-order transitions found at $T=0$.

E. Effect of electron and phonon degeneracy

Nondegenerate phonons. The effect of electron spin and orbital degeneracy on models with scalar phonons is straightforward, if there is no long-range order. One multiplies the quantity $\text{Tr} \ln[G_{\text{eff}}^{-1}]$ in Eq. (6) by the factor $n_{\text{spin}} n_{\text{orb}}$. This factor may be absorbed into T and g by defining $T = T n_{\text{spin}} n_{\text{orb}}$, and $g = g / \sqrt{n_{\text{spin}} n_{\text{orb}}}$ and the model reduces to the previous case, apart from small differences coming from the T dependence of the Fermion action. This is shown in Fig. 5, which depicts $\rho(T)$ for a model with a twofold electron degeneracy ($n_{\text{spin}} n_{\text{orb}} = 2$). The couplings are chosen to differ by a factor of $\sqrt{2}$ from those used to construct Fig. 3, so as to produce the same $T=0$ behavior. The resistivity is smaller by a factor of 2, because it is proportional to $1/n_{\text{orb}} n_{\text{spin}}$. If the temperature axis is rescaled by a factor of two, the various curves lie almost on top of each other, with agreement being best for low- T and weak coupling. For example, the temperatures at which the resistivity turns up for $g=1.83$ and 1.69 in the nondegenerate case are almost exactly one-half of the temperatures at which ρ turns up for $g=1.30$ and 1.20 . Some deviations from this scaling become apparent at higher T ; these are due to the T dependence of the Fermion action (i.e., to the electron entropy). For example, the scaled weak coupling resistivities differ by an amount proportional to T^2 . Similarly, the upturn for the strongest coupling occurs at a slightly lower rescaled temperature in the degenerate case. Again for $g \gg g_c$ the model is

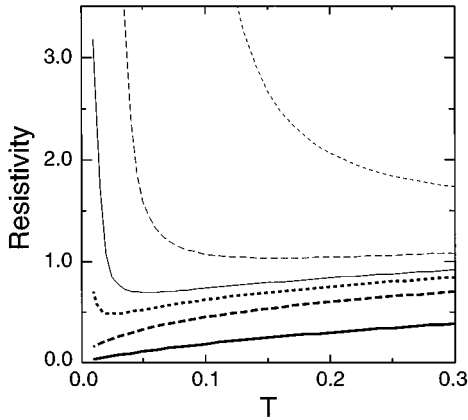


FIG. 5. Temperature (T) dependence of resistivity (ρ) for model of degenerate electrons and nondegenerate phonons with $n=1$ and $g=0.91$ (heavy solid line), 1.09 (heavy dashed line), 1.13 (heavy dotted line), 1.15 (light solid line), 1.20 (light dashed line) and 1.30 (light dotted line). These couplings produce the same $T=0$ gaps as in Fig. 2. The factor of $\sqrt{2}$ in the couplings and the factor of 2 in the resistivity relative to Fig. 2 come from orbital degeneracy.

insulating as $T \rightarrow 0$. The approach to the $T \rightarrow 0$ limit for this model is shown in the middle panel of Fig. 6. It is seen that in this model our calculations can access more of the low T limit because of the rescaling of the temperature.

Degenerate phonons Jahn-Teller coupled to orbitally degenerate electrons. The theory is based on Eq. (5); signifi-

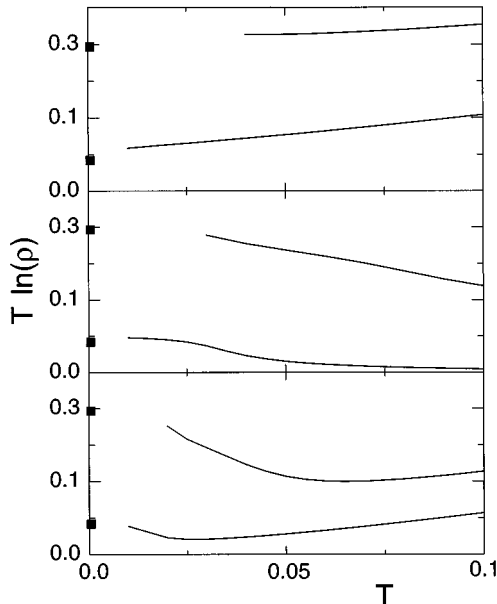


FIG. 6. Low-temperature behavior of resistivity (ρ) for the three models considered in the text for parameters such that the spectral function has a gap at $T=0$: lower panel: nondegenerate phonons and nondegenerate electrons, middle panel: nondegenerate phonons and degenerate electrons, upper panel: degenerate phonons and degenerate electrons. The expected low- T behavior is $\rho \sim T^\alpha e^{\Delta/T}$ with Δ the low- T gap in the spectral function. The heavy dots mark values of Δ obtained from an analytic $T=0$ calculation as described in the text.

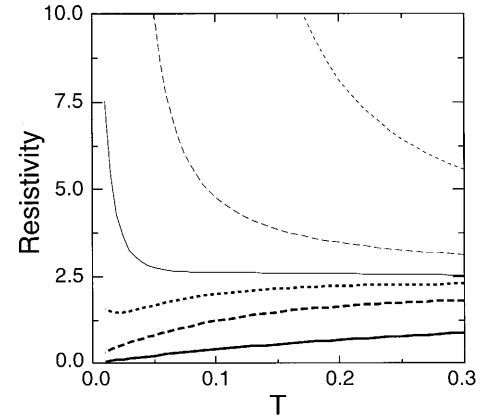


FIG. 7. Temperature (T) dependence of resistivity (ρ) for model of degenerate electrons and degenerate phonons with $n=1$ and $g=0.91$ (heavy solid line), 1.09 (heavy dashed line), 1.13 (heavy dotted line), 1.15 (light solid line), $g=1.20$ (light dashed line), and 1.30 (light dotted line). These couplings produce the same $T=0$ gaps as in Figs. 2 and 5. Note ρ is much larger than that shown in Fig. 5 for the nondegenerate electrons model, reflecting the stronger scattering.

cant differences from the previous cases occur because the electron spectral function may have a more complicated structure and the phonon measure suppresses the probability of small amplitude lattice distortions and increases the probability of large amplitude distortions.

We begin with the effect of the phonon measure. For this discussion we restrict our attention to $n=1$, so the only difference in the model is the factor of rdr in the phonon measure. Figure 7 shows the resistivity of this model for $n=1$ at the same coupling constants used to construct Fig. 5. One sees immediately that all resistivities are larger in the Jahn-Teller case; also for parameters such that there is a $T=0$ gap, up-turns occur at higher-temperatures. The origin of these differences may be seen most easily in the phonon probability distribution $P(x)$, shown in Fig. 8 for both degenerate and nondegenerate phonons using in both cases degenerate electrons. We have chosen $g=g_c=1.085$ (the critical value at which the $T=0$ lattice distortion vanishes) and $T=0.15$. The results are representative of all g and T . One sees immediately that the mean square value of the lattice displacement is larger in the Jahn-Teller case than in the nondegenerate case and more importantly the small r fluctuations are suppressed. The larger mean square displacement means more scattering and hence more resistivity. The suppression of small r fluctuations means that $P(r)$ is reasonably sharply peaked at a nonzero value, $r=r_{\text{peak}}$. The temperature-dependence of r_{peak} in the degenerate-phonon case is determined by the coupling; for $g < g_c$ $r_{\text{peak}}(T) \sim T^{1/2}$, for $g = g_c$ $r_{\text{peak}}(T) \sim T^{1/4}$ and for $g > g_c$ r_{peak} tends to a constant.

For nondegenerate phonons and $T=0$, $P(r)$ has a maximum at $r=0$ if $g < g_c$ and maxima at $r \neq 0$ if $g \geq g_c$. Even for $g < g_c$ $P(r)$ at $T \neq 0$ may have a weak maximum at $r \neq 0$, but this does not seem to have any consequences for physical properties. In the degenerate-phonon case the peak structure of $P(r)$ actually can lead to a minimum in the spectral function at zero frequency if $g r_{\text{peak}}$ exceeds a critical value somewhat larger than the 0.5 value found in Appendix

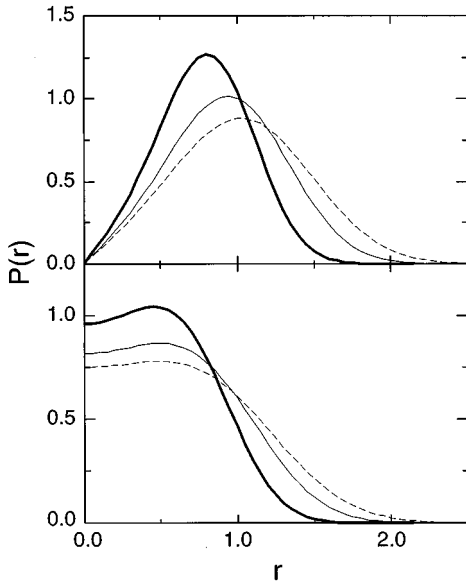


FIG. 8. Lower panel: phonon probability distribution $P(r)$ for $g=1.085$, $n=1$, $T=0.05$ (heavy solid line), 0.1 (light solid line), and 0.15 (light dashed line) and nondegenerate phonons. Upper panel: phonon probability distribution $P(r)$ for same parameters and degenerate phonons.

C. Of course if $g \leq g_c$, this minimum will vanish as T is decreased. This behavior is illustrated in Fig. 9, which shows the temperature evolution of the spectral functions for the two models. Only the degenerate phonon case has a minimum at $\omega=0$; the minimum vanishes below $T \sim 0.045$, at which temperature $gr_{\text{peak}} \sim 0.5$. This may be understood by reference to the $T=0$ limit, in which $P(r)$ may be approximated by a δ function at a coupling dependent value r_0 . If $gr_0 > 0.5$ the $T=0$ spectral function develops a minimum at $\omega=0$; if $gr_0 > 1$ it develops a gap. Similarly, at $T > 0$ the

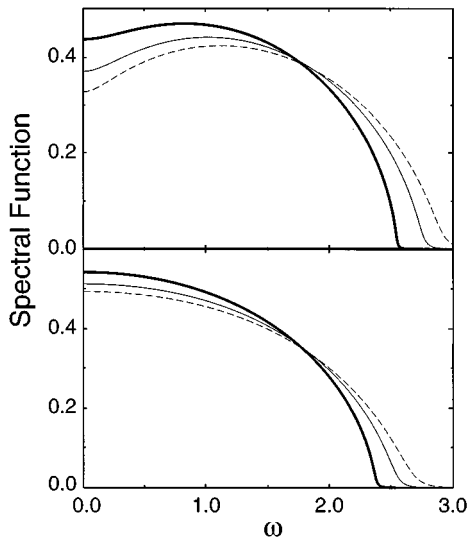


FIG. 9. Comparison of temperature evolution of electron spectral functions for degenerate (upper panel) and nondegenerate (lower panel) phonons and orbitally degenerate electrons for $n=1$ and $g=1.085$, $T=0.05$ (heavy solid line), 0.1 (light solid line), and 0.15 (light dashed line) as used in Fig. 8.

peak in the degenerate-phonon $P(r)$ leads to a minimum in $A(\omega)$ if this peak occurs at an r_{peak} such that $gr_{\text{peak}} > 0.5$. This tendency to open or increase a gap in the electron spectral function as T is raised acts to increase the resistivity of the degenerate model above that of the nondegenerate one.

Finally, the approach to the $T \rightarrow 0$ limit for the insulating regime is shown in the upper panel of Fig. 6. It is interesting that the result approaches the $T \rightarrow 0$ limit more smoothly than in the two previous cases, and also that $T \ln \rho$ is larger at $T > 0$ than at $T=0$, unlike the other two cases. We speculate that the origin of this difference is the larger rms value of r , which would imply an effectively larger gap.

Away from $n=1$ a more important difference in physics occurs, which is most easily seen for spinless electrons in the very strong coupling limit. Suppose $n < 1$ and neglect hopping completely. Then by analogy with the steps leading to Eq. (42) one expects n sites occupied by a single electron and $1-n$ unoccupied. The spectral function associated to the singly occupied sites has two peaks, one below the chemical potential corresponding to the occupied orbital and one above corresponding to the unoccupied orbital. The spectral function associated with the unoccupied sites has only one peak, because in the absence of any electrons there is no lattice distortion and therefore no splitting of the orbitals. The spectral function thus has a three-peak structure in the strong coupling limit.

Consider now the first perturbative correction due to the hopping. This will lead to a charge-density $\delta n \sim n/\lambda$ on previously unoccupied sites. If (as assumed in our application of the dynamical mean-field method) there are no intersite correlations in orbital occupancy or phonon fluctuations, this extra charge will be randomly distributed over the two on-site orbitals. Thus in the presence of a small amplitude phonon distortion δr the charge fluctuation will lead to an energy gain of at most $\delta n (\delta r)^2$, which will be too weak to compete with the phonon stiffness in the strong coupling limit. The three-peaked spectral function is therefore stable in the strong coupling limit. Appendices D and E derive these results from an asymptotic analysis of the dynamical mean-field equations. It is clear from the above arguments that the structure of the midgap states may be affected by intersite correlations, which could lead to a charge fluctuation favoring one particular orbital, and therefore to an energy gain proportional to δr rather than δr^2 . Incorporating intersite correlations is an important open problem. Of course, as λ is decreased, the possible energy gain increases and at some point the midgap states split and the two pieces join the upper and lower bands. The resulting intermediate coupling regime corresponds to a uniform electron density and a uniform nonzero lattice distortion. The electron spectral function consists of two bands, with the Fermi level in the lower one (for $n < 1$). The rigid bandlike state gains kinetic energy $\sim 1-n$ relative to the three-band state, because one band is not fully filled, but is shown in Appendices D and E to be more costly in Jahn-Teller energy because the lattice distortion is not as large.

Thus, as the coupling is increased at $T=0$ three phases are in principle possible: a weak coupling phase with a single-peaked spectral function, a ‘‘rigid band’’ phase with a two-peaked spectral function and the Fermi level in the lower band, and an insulating three-peaked spectral function.

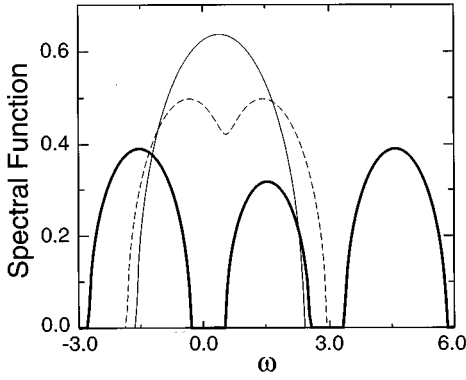


FIG. 10. Evolution of $T=0$ spectral function with coupling strength. Model with degenerate electrons, degenerate phonons, and $n=0.75$ for coupling constants $g=1.53$ (light solid line), 1.58 (light dashed line), and the strong coupling limit solution evaluated at $g=2.47$ (heavy solid line).

Determining the couplings at which the system goes from one phase to another in general requires numerical solution of the coupled mean-field equations, along with comparison of the energies of different locally stable solutions. However, in the limit $(1-n) \rightarrow 0$ the equations simplify and a straightforward physical argument may be used. Consider the $n=1$ problem in the insulating regime in which the spectral function has two peaks separated by a gap and calculate the electron removal spectrum allowing the on-site lattice distortion to adjust. (The $\omega < 0$ part of the spectral function previously computed for this problem represents the lowest-energy way to remove an electron from the system at fixed lattice distortion.) This energy may be computed from the quantity $G_{ii}^{ab}(\omega, r)$ defined in Eq. (19), with the G on the right-hand side of the equation given by the $n=1$ solution of the dynamical mean-field equations. Performing this computation and optimizing over r shows that there are two extrema—one at $r=0$ and one at $r=r^*$ (with r^* the optimum r found for $n=1$). If $g > 1.308, \dots$ (i.e., $r^* > 1.527, \dots$) then the energy of the $r=0$ extremum is lower, showing that the three-peaked spectral function is favored, while for $g < 1.308, \dots$ the ‘rigid band’ solution is favored. (Note that at $g=1.308$ the two peaks of the rigid band spectral function are separated by a gap.) For this reason we believe that for $1-n \ll 1$ there is as g is increased a second-order transition to the rigid band two-peaked spectral function. As g is increased further, the peaks separate and eventually a gap develops between them (although the ground state remains conducting). This is followed by a first-order transition at a larger g to an insulating state with a three-peaked spectral function. This sequence of spectral functions is shown in Fig. 10. On the other hand, for $n \rightarrow 0$ the results of Appendix E show that the weak coupling one-peak spectral function proceeds directly to the three-peaked one via a first-order transition.

One important consequence of the central feature appearing in the three-peak regime is that it acts to fill in the gap created by the lattice distortion, so that one must go to stronger couplings and lower temperatures to see insulating behavior in the Jahn-Teller case than in the nondegenerate case. This may be seen directly from the strong coupling calculations of Appendices C and E. In the nondegenerate case the

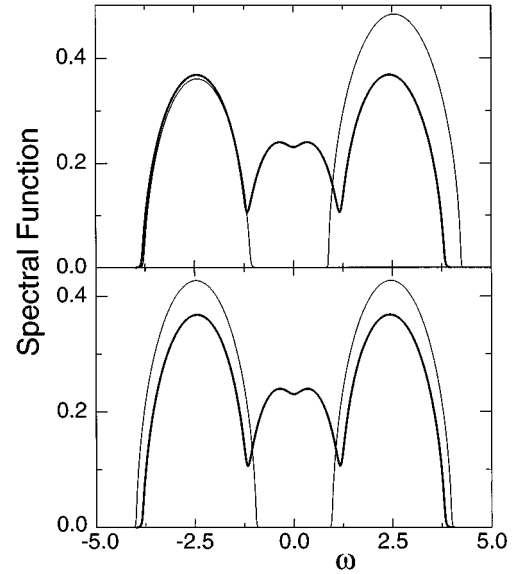


FIG. 11. Comparison of low- T spectral functions. Upper panel: Jahn-Teller (heavy line, shifted by $\mu = -1.23$) and nondegenerate phonons (light line) at $T=0.03$, $g=1.58$, and $n=0.75$. Lower panel: $n=1$ (light) and $n=0.75$ (heavy) with Jahn-Teller phonons, $T=0.03$ and $g=1.58$. $n=0.75$ curve (heavy line) shifted by $\mu = -1.23$.

spectral function has two features, at $\pm g^2$ and physical quantities are controlled by the energy gap between them, which is of about the same size. In the Jahn-Teller case the highest and lowest of the three peaks are still separated by an energy of $2g^2$, but physical processes are controlled by the gap separating the lowest and middle peaks, which is much less. This may also be seen in numerical calculations of the low- T spectral functions and phonon probability distributions. The upper panel of Fig. 11 compares the spectral functions for the nondegenerate and Jahn-Teller cases at $T=0.03$, $g=1.58$, and $n=0.75$. Although the true $g > 1$ strong coupling limit has not been reached, the two-peaked and three-peaked structures expected for the nondegenerate and Jahn-Teller cases are clearly visible and the gap in the Jahn-Teller case is much less. Similarly, the lower panel compares the spectral functions for $n=1$ and $n=0.75$, for $g=1.58$, $T=0.03$, and Jahn-Teller coupling. Again one sees the effect of the midgap states. Figure 12 similarly compares the phonon probability distributions in the two cases. Figure 13 compares the resistivities of the two models for the weaker coupling $g=1.29$; the nondegenerate phonon model displays insulating behavior below $T \sim 0.13$, while the Jahn-Teller model remains metallic. The resistivities cross at higher T because of the larger fluctuations of $\langle r^2 \rangle$ in the Jahn-Teller case.

V. CONCLUSIONS

We have used the dynamical mean-field method to study the crossover from Fermi liquid to polaron behavior in models of electrons coupled to localized classical phonons. The models we studied involved electrons with and without spin and orbital degeneracy coupled to degenerate and nondegenerate phonons. We considered two forms of electron-phonon

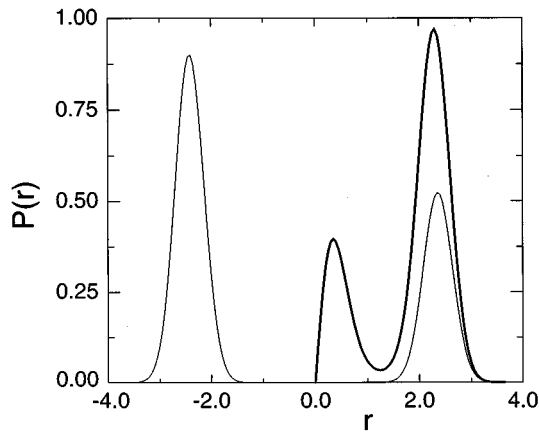


FIG. 12. Comparison of low- T phonon probability distribution $P(r)$ for Jahn-Teller (heavy line) and nondegenerate (light line) phonons for $T=0.03$, $g=1$, and $n=0.75$. Note that the large r peaks occur at almost exactly the same r . Note also that the Jahn-Teller $P(r)$ is defined only for $r>0$. The asymmetry in $P(r)$ in the nondegenerate case is a consequence of particle hole asymmetry due to $n \neq 1$.

coupling: conventional, in which the phonon displacement couples to the electron charge-density, and Jahn-Teller, in which the phonon displacement couples to the splitting of the electronic levels. We showed that as $T \rightarrow 0$ three regimes may be distinguished. In *weak coupling* the mean square displacement of the oscillator coordinate from its noninteracting reference position vanishes and the momentum-integrated electron spectral function assumes the noninteracting form. Corrections lead to the usual linear T resistivity. In *intermediate coupling* the mean square displacement of the oscillator coordinate is nonvanishing and the spectral function is changed from its noninteracting form, but the density of states at the Fermi level is nonzero so the $T \rightarrow 0$ resistivity is neither zero nor infinite. In *strong coupling* the mean square displacement is nonvanishing and is sufficiently large that a gap appears in the spectral function and the resistivity diverges as $T \rightarrow 0$. Examples of the evolution of the $T=0$ momentum-integrated spectral function with coupling strength are shown in Figs. 1 and 10. Figure 1 is calculated

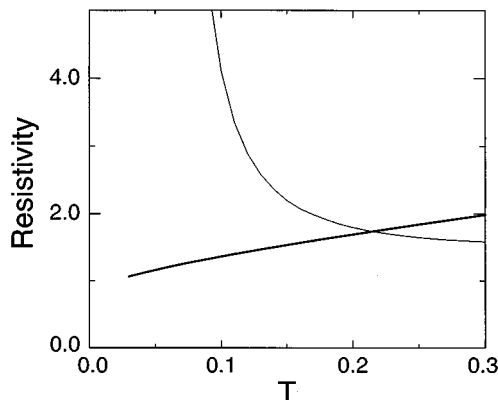


FIG. 13. Comparison of temperature-dependent resistivities for Jahn-Teller (heavy line) and nondegenerate phonons (light line), $g=1.29$ and $n=0.75$.

for the simplest model at half filling, but the results at any filling for any model involving coupling of the oscillator to the charge-density of the electrons are similar. The only important effects are that away from half filling in the strong coupling limit the relative weights of the two peaks are different and that there is at $T=0$ a discontinuous, rather than continuous, change in the spectral function and $\langle r^2 \rangle$ as the coupling is increased. We believe, but have not proven, that at any $T>0$ the change is continuous. The evolution of the spectral function for the case of Jahn-Teller coupling is shown in Fig. 10. The significant difference is the presence of the midgap feature in the strong coupling limit. This has relative weight $|2-2n|$ and corresponds physically to sites unoccupied by electrons. This midgap feature means that for Jahn-Teller couplings and $n \neq 1$ the gap controlling physical properties is much smaller at given coupling than it is in models in which the phonon is coupled to the charge-density, and the midgap state is absent.

Three physical effects have been left out of our calculation. One is the on-site Coulomb repulsion, which is certainly important in transition metal oxides. The Coulomb interaction tends to localize electrons, with the effect being strongest at commensurate fillings and so will tend to reinforce the localizing effect of the electron-phonon interaction. Because the localizing effect of the Coulomb interaction is strongest at commensurate fillings, this will also lead to an interesting doping dependence: the effective electron-phonon coupling will weaken as n is varied from 1. The Coulomb interaction will also change the form of the spectral function, because it raises the energy of states with two electrons on the same site. For example, the uppermost peak of the strong coupling spectral function shown in Fig. 10 corresponds physically to the density of states for adding an electron to a site with one electron already present, at fixed phonon configuration. Coulomb effects will shift this energy upwards. A quantitative treatment of these effects within the present formalism will be left to a future paper.

A second important piece of physics is quantum fluctuations of the phonons. At low-temperatures and in the absence of long-range order, these will allow electrons to move from site to site even in the strong coupling regime, thus cutting off the strong-coupling divergence in the resistivity. One mathematical consequence is the appearance of Gaussian tails to the spectral functions in the gap regions.

A third omitted piece of physics is long-range order. It has been assumed throughout that the lattice distortions are random from site to site; thus the localization is due purely to polaronic effects. Near commensurate densities, charge-density-wave effects will be important as well.

ACKNOWLEDGMENTS

We thank J. Freericks, B. G. Kotliar, P. B. Littlewood, and A. Sengupta for helpful discussions. R.M. was supported in part by the Studienstiftung des Deutschen Volkes.

APPENDIX A: RELATION TO MIGDAL-ELIASHBERG THEORY

In this Appendix we derive the relationship between the formalism we have used and the conventional Migdal-Eliashberg theory of the weakly coupled electron-phonon

system. The essential parameter of the conventional treatment is a dimensionless coupling constant λ_{conv} , which is defined in terms of the electron self-energy $\Sigma(\omega, T)$ via

$$\lim_{\omega \rightarrow 0} \frac{\partial \Sigma(\omega, T=0)}{\partial \omega} = \lambda_{\text{conv}}. \quad (\text{A1})$$

To establish the relationship we introduce a finite phonon mass M_{ph} . This implies a Debye frequency ω_D given by

$$\omega_D^2 = k/M_{\text{ph}} a^2 \quad (\text{A2})$$

with a the lattice constant. (We use units in which $\hbar = 1$.) We then introduce phonon creation and annihilation operators b^\dagger, b via

$$r = (b^\dagger + b)/(2M_{\text{ph}}\omega_D)^{1/2}. \quad (\text{A3})$$

Comparison to Eq. (4) yields

$$H_{\text{el-ph}}^{\text{conv}} = \left(\frac{g^2}{2M_{\text{ph}}\omega_D} \right)^{1/2} \sum_{i\alpha} (d_{i\alpha}^\dagger d_{i\alpha} - n)(b_i^\dagger + b_i). \quad (\text{A4})$$

The standard electron-phonon calculation gives

$$\frac{\partial \Sigma(\omega, T=0)}{\partial \omega} = n_{\text{orb}} n_{\text{spin}} \frac{g^2}{k} \mathcal{D}(\epsilon_F), \quad (\text{A5})$$

where $\mathcal{D}(\epsilon_F)$ is the single-spin density of states at the Fermi surface. Thus

$$\lambda_{\text{conv}} = t \mathcal{D}(\epsilon_F) \lambda. \quad (\text{A6})$$

Elsewhere in this paper it has been shown that in the dynamical mean-field calculations polaron effects occur at $\lambda \sim 1$, implying $\lambda_{\text{conv}} \sim 1$. For example, in the model with $n_{\text{orb}} = n_{\text{spin}} = 1$ and a semicircular density of states at $\mu = 0$, frozen phonon distortions begin to occur at $\lambda = \pi$ ($\lambda_{\text{conv}} = 1$). The critical values of λ found here are artificially small because of neglect of quantum fluctuations and intersite interactions. In models with quantum phonons, somewhat larger λ values will be required to produce insulating behavior, but the general conclusion that metallic behavior breaks down at a λ_{conv} not too much larger than 1 will still hold. Now Migdal showed, using phase-space arguments, that the parameter that controls perturbation theory about the zero electron-phonon coupling limit is not λ but $\lambda \omega_D/t$ (or if $T > \omega_D$, $\lambda T/t$).⁴ Therefore, one might expect to be able to use the Migdal-Eliashberg equation to study the crossover from Fermi liquid to polaron physics. The difficulty with this argument, however, is that the ground state about which to perform the expansion is not known for $\lambda > 1$. In fact, in the limit considered in this paper, the Migdal-Eliashberg equations are identical to those obtained by expanding Eq. (6) to order r^2 and solving self-consistently. Corrections to this self-consistent solution are indeed small, if $\lambda T/t$ is small, but the starting point is seen to be wrong if $\lambda > \lambda_c \approx 1$. That the Migdal approximation breaks down at $\lambda \sim 1$ has been noted by other workers; see, e.g., Alexandrov, Kabanov, and Ray.³

APPENDIX B: NONDEGENERATE FERMIONS WITH LORENTZIAN DENSITY OF STATES

In this Appendix we use steepest-descent techniques to analyze the $T \rightarrow 0$ limit of the dynamical mean-field theory of spinless Fermions with a Lorentzian density of states coupled to a scalar classical oscillator. A similar technique was used in Ref. 5. The partition function is

$$Z(g, n) = \int dr e^{-E(r, g, n)/T}. \quad (\text{B1})$$

The energy $E = -T \ln P(r)$ with $P(r)$ defined in Eq. (11); it may be evaluated by inserting Eqs. (17) and (10) into Eq. (11). One finds

$$E(r, g, n) = \frac{1}{2} r^2 - g r n - [\mu - g r] \left[\frac{1}{2} + \frac{1}{\pi} \tan^{-1}(\mu - g r) \right] + \frac{1}{2\pi} \ln[1 + (\mu - g r)^2] + \mu n + OT^2. \quad (\text{B2})$$

with the chemical potential μ chosen so that

$$dZ/d\mu = 0. \quad (\text{B3})$$

As $T \rightarrow 0$, the r integral is dominated by the values r^* minimizing E . We have

$$Z(g, n) \rightarrow \sum_a Z_a \exp -E(r_a^*, g, n)/T. \quad (\text{B4})$$

Here a labels the extrema, r_a^* is a solution of

$$r = g \left(n - \frac{1}{2} - \frac{1}{\pi} \tan^{-1}(\mu - g r) \right), \quad (\text{B5})$$

and $Z_a \geq 0$ is the weight associated with extremum a . Each Z_a is a product of two contributions, one from integrating over the quadratic fluctuations in r about $r = r_a^*$ and one from the leading T dependence of μ . In the present problem we have, at low T , $\mu = \mu_0 + AT$; the T -linear term contributes to Z_a .

Equation (B5) may have one or three solutions. In the latter case, either one has the lowest energy or two are degenerate. If there is one dominant extremum then Eq. (B3) implies

$$\mu = g r + \tan \pi(n - 1/2), \quad (\text{B6})$$

so Eq. (B5) implies $r = 0$.

Now consider the case of two degenerate extrema, at $r = r_1$ and $r = r_2$. From Eq. (B3) and Eq. (B5) one finds $Z_1 r_1 + Z_2 r_2 = 0$; as $Z_{1,2} \geq 0$, r_1 and r_2 must have opposite signs. It is convenient to define

$$R = g(r_1 + r_2)/2, \quad \Delta = g(r_1 - r_2)/2. \quad (\text{B7})$$

In terms of these variables Eq. (B5) become

$$R = g^2(n - 1/2) - \frac{g^2}{2\pi} \tan^{-1} \frac{2\mu - 2R}{1 - (\mu - R)^2 + \Delta^2}, \quad (\text{B8})$$

$$\Delta = \frac{g^2}{2\pi} \tan^{-1} \frac{2\Delta}{1 + (\mu - R)^2 - \Delta^2}. \quad (\text{B9})$$

These equations must be solved subject to the constraint $E(r_1, g, n) = E(r_2, g, n)$, which by use of Eqs. (B8) and (B2) may be written

$$(R - \mu)\Delta = \frac{g^2}{4\pi} \ln \frac{1 + (R - \mu + \Delta)^2}{1 + (R - \mu - \Delta)^2}. \quad (\text{B10})$$

At small R and Δ , Eqs. (B10) and (B9) are only consistent if $R = \mu = g^2(n - 1/2)$, so (B10) is trivial. This may be most easily seen by expanding the two equations in Δ at fixed $\mu - R$ and comparing the Δ^3 coefficients. This immediately implies that if $n \neq 1/2$ the transition is first order.

In the strong coupling limit, $r_1 = -g(1 - n)$, $r_2 = gn$ and $\mu = \frac{1}{2}g^2(n - 1/2)$. One may obtain Eq. (44) by substituting the value for, e.g., r_2 and μ into Eq. (B2).

APPENDIX C: NONDEGENERATE FERMIONS WITH SEMICIRCULAR DENSITY OF STATES

In this Appendix we analyze the $T \rightarrow 0$ limit of the dynamical mean-field theory of nondegenerate Fermions with a semicircular density of states coupled to a classical oscillator. The technical differences from the Lorentzian case treated in Appendix B are that the mean-field parameter satisfies the self-consistency equation (18) and that the energy is given by

$$E(r, g, n) = -\frac{1}{2}T \sum_n [a_n - (i\omega_n + \mu)]^2 + \frac{r^2}{2} - grn - T \sum_n \ln[a_n - gr] + \mu n, \quad (\text{C1})$$

with r given by a solution of

$$r = g \left(n + \sum_n \frac{1}{a_n + gr} \right). \quad (\text{C2})$$

If there is one dominant extremum then Eqs. (B4) and (18) imply $n = -\sum_n (a_n + gr)^{-1}$ so Eq. (C2) implies $r = 0$. In this case

$$a(i\omega_n) = \frac{1}{2}[(i\omega_n + \mu) - \text{sgn}\omega_n \sqrt{(i\omega_n + \mu)^2 - 4}]. \quad (\text{C3})$$

If there are two degenerate extrema, Eqs. (B4), (B7) apply, as do the relations $Z_1 r_1 + Z_2 r_2 = 0$ and $E(r_1, g, n) = E(r_2, g, n)$ used in Appendix B. It is convenient to rewrite the equations in terms of R, Δ , $b_n = a_n + R$, and $z_n = i\omega_n + \mu + R$ as

$$R = g^2 n + g^2 T \sum_n \frac{b}{(b^2 - \Delta^2)}, \quad (\text{C4})$$

$$\Delta = -g^2 T \sum_n \frac{\Delta}{(b^2 - \Delta^2)}, \quad (\text{C5})$$

$$2R\Delta = 2g^2 n \Delta + g^2 T \sum_n \ln \frac{b + \Delta}{b - \Delta}, \quad (\text{C6})$$

$$b = z - \frac{b + R}{b^2 - \Delta^2}. \quad (\text{C7})$$

For $n \neq 1/2$, the transition may be shown to be first-order by the argument used in Appendix B: one expands Eqs. (C5) and (C6) to order Δ^3 at fixed b and R and observes that the equations are not compatible.

For $n = 1/2$, $\mu = R$ and b is odd in $i\omega_n$, so Eqs. (C4) and (C6) are satisfied trivially. The other two equations may be easily solved by viewing them as equations for b and g^2 at given Δ . Because Eq. (C7) is only cubic, the solution may be written down immediately. It is easiest to find the proper branch of the solution if z is continued to the real axis. Once b is found, g^2 may easily be computed from Eq. (C5). From Eq. (C7) one sees immediately that the imaginary part of b, b'' , vanishes at $\omega = 0$ for $\Delta^2 = 1$. The coupling corresponding to this, $g = 1.63$, is the one at which a gap first appears in the spectrum. Similarly, one may show that the leading (ω^2) correction to the $\omega = 0$ value of b'' vanishes at $\Delta^2 = 1/4$.

The strong coupling limit is analytically tractable at all n . b'' is nonzero only for Z near $\pm \Delta$. Defining $b_{\pm} = b \pm \Delta$ and $Z_{\pm} = Z \pm \Delta$ and neglecting terms of order $1/\Delta$ one finds from Eq. (C7)

$$b_{\pm} \cong Z_{\pm} - \frac{1}{2b_{\pm}}(1 \pm R/\Delta). \quad (\text{C8})$$

This equation may be solved and the results inserted into the other equations. One finds

$$r_1 = -g(1 - n), \quad r_2 = gn, \quad \mu = g^2(n - 1/2). \quad (\text{C9})$$

The physical content of these solutions is one band, of width $\sqrt{2n}$ centered at $\omega = -g^2$ representing occupied states and another at $\omega = g^2$ of width $\sqrt{2(1 - n)}$ representing unoccupied states.

APPENDIX D: ORBITALLY DEGENERATE ELECTRONS WITH LORENTZIAN DENSITY OF STATES

In this Appendix we analyze the $T \rightarrow 0$ limit of the dynamical mean-field theory of orbitally degenerate electrons with a Lorentzian density of states coupled to a classical Jahn-Teller oscillator whose displacement has magnitude r . The treatment parallels Appendix B but the details are different. Instead of (B2) we have

$$E(r, g, n) = \frac{1}{2}r^2 - (\mu + gr) \left(\frac{1}{2} + \frac{1}{\pi} \tan^{-1}(\mu + gr) \right) - (\mu - gr) \left(\frac{1}{2} + \frac{1}{\pi} \tan^{-1}(\mu - gr) \right) + \frac{1}{2\pi} \ln[1 + (\mu + gr)^2] + \frac{1}{2\pi} \ln[1 + (\mu - gr)^2] + \mu n$$

with μ chosen so (B3) holds. Instead of Eq. (B5) we have

$$r = \frac{g}{\pi} [\tan^{-1}(\mu + gr) - \tan^{-1}(\mu - gr)]. \quad (\text{D1})$$

Suppose first there is only one dominant extremum. If g is small this is at $r=0$ and

$$\mu = \tan\frac{\pi}{2}(n-1) \quad (\text{D2})$$

and

$$E(r=0, n) = -\frac{2}{\pi} \ln\left(\cos\frac{\pi}{2}(n-1)\right). \quad (\text{D3})$$

At $g = g_c(\mu) = 2/[\pi(1 + \mu^2)]$, there is a second-order transition to a state with $r \neq 0$. In this state, the chemical potential is fixed by

$$n = 1 + \frac{1}{\pi} [\tan^{-1}(\mu + gr) + \tan^{-1}(\mu - gr)]. \quad (\text{D4})$$

As $g \rightarrow \infty$ at $n \leq 1$, this solution tends to $r = \pm gn$, $\mu = \tan\pi(n-1/2) - g^2n$, $E = -\frac{1}{2}g^2n^2 + (1/\pi)\ln g^2n$.

At large g and $n \neq 1$, Eq. (D1) has an alternative solution, $r = g$. This is incompatible with Eq. (D4), so the solution must be degenerate with another extremum, which, by symmetry, must be at $r=0$. These requirements imply that $\mu = \frac{1}{2}g^2 \text{sgn}(n-1)$ and $E \rightarrow -\frac{1}{2}g^2n + (4/\pi)\ln g$. If n is near 1 the two-extremum solution becomes lower in energy at $g \sim 1/\sqrt{1-n} \gg g_c$; if n is near 0, the two-extremum solution is lower in energy at all $g > g_c$.

APPENDIX E: JAHN-TELLER COUPLED ELECTRONS WITH SEMICIRCULAR DENSITY OF STATES

In this Appendix we analyze the $T \rightarrow 0$ limit of the dynamical mean-field theory of orbitally degenerate electrons with a semicircular density of states coupled to a classical Jahn-Teller oscillator whose displacement has magnitude r . The treatment follows Appendix C but with technical differences analogous to those found in Appendix D. Instead of Eq. (C1) we have

$$E(r, g, n) = T \sum_n [a_n - (i\omega_n + \mu)]^2 + \frac{1}{2}r^2 - T \sum_n \ln[a_n^2 - g^2r^2] + \mu n. \quad (\text{E1})$$

Instead of Eq. (C2) we have

$$r = -2g^2rT \sum_n \frac{1}{a_n^2 - g^2r^2}. \quad (\text{E2})$$

If there is one dominant extremum then a satisfies

$$a_n = i\omega_n + \mu - \frac{a_n}{a_n^2 - g^2r^2} \quad (\text{E3})$$

while μ is given by

$$n = 2T \sum_n \frac{a_n}{a_n^2 - g^2r^2}. \quad (\text{E4})$$

For small g , the only possible solution is $r=0$, so a_n is given by Eq. (18) and μ may be found numerically from Eq. (E4). The $r=0$ solution becomes linearly unstable at

$$g_c^2(\mu) = 3\pi/(4 - \mu^2)^{3/2} \quad (\text{E5})$$

to a solution with $r \neq 0$. This solution implies a frozen in Jahn-Teller splitting randomly oriented from site to site but of the same magnitude on all sites, and therefore a two-peaked spectral function. Again the equations simplify in the strong coupling limit, where the reasoning that led to Eq. (C8) shows that the single-extremum solution tends to one with a spectral function consisting of two semicircular features of half-width $\sqrt{2}$ (versus half-width 2 at $g < g_c$), centered at $\omega = -\mu \pm g^2$. For $n < 1$ μ is such that the lower band is partly filled, thus $\mu = -g^2n + O(1)$, and the energy is $-\frac{1}{2}g^2n^2 + O(1-n)$. The $O(1-n)$ term comes from carrier kinetic energy in the partly filled band.

As in Appendix D, an alternate two-extremum solution exists, with one extremum at $r=0$ and the other at $r \neq 0$. As $g \rightarrow \infty$, the nonzero $r \rightarrow g$. The spectral function consists of three well separated peaks; two each of weight $\min(n, 2-n)$, at $\omega - \mu = \pm g$ corresponding to sites with an electron and one, of weight $2|1-n|$, centered at $\omega = -\mu$ and corresponding to the empty sites if $n < 1$ and the doubly occupied sites at $n > 1$. The chemical potential is $-\frac{1}{2}g^2$ and the energy is $-\frac{1}{2}g^2n + O(1/g)$. As $g \rightarrow \infty$ the two extremum solution is lower in energy. For $n \rightarrow 0$, $\mu \rightarrow -2$ in the undistorted state and the divergence of g_c shown in Eq. (E5) implies that the undistorted state proceeds directly to the three-peaked one via a first-order transition. For n near 1 the calculation sketched in the text shows that the two-peaked solution, with a gap between the two peaks, exists for a finite range of g .

¹A. Georges, B. G. Kotliar, W. Krauth, and M. J. Rozenberg, *Rev. Mod. Phys.* **68**, 13 (1996).

²A. J. Millis, R. Mueller, and B. I. Shraiman, following paper, *Phys. Rev. B* **54**, 5405 (1996).

³See, e.g., Chaps. 4 and 6 of G. D. Mahan, *Many Particle Physics*, (Plenum, New York, 1981) and references therein, and for more recent work see, e.g., A. S. Alexandrov, V. V. Kabanov, and D. K. Ray, *Phys. Rev. B* **49**, 9915 (1994), and references therein.

⁴A. B. Migdal, *Zh. Éksp. Teor. Fiz.* **34**, 1438 (1958) [*Sov. Phys. JETP* **7**, 996 (1958)].

⁵R. T. Scalettar, N. E. Bickers, and D. J. Scalapino, *Phys. Rev. B* **40**, 197 (1989).

⁶J. Freericks, M. Jarrell, and D. J. Scalapino, *Phys. Rev. B* **48**, 6302 (1993).

⁷M. Jarrell and D. J. Scalapino, *Phys. Rev. B* **48**, 6302 (1993).

⁸C. Grimaldi, L. Pietronero, and S. Strassler, *Phys. Rev. Lett.* **75**, 1158 (1995).

⁹J. K. Freericks, *Phys. Rev. B* **48**, 3881 (1993).

¹⁰E. D. Wollan and W. C. Koehler, *Phys. Rev.* **100**, 545 (1955); G. Matsumoto, *J. Phys. Soc. Jpn.* **29**, 613, (1970).

¹¹S. Jin, T. H. Tiefel, M. McCormack, R. A. Fastnacht, R. Ramesh, and L. H. Chen, *Science* **264**, 413 (1994).

¹²A. J. Millis, P. B. Littlewood, and Boris I. Shraiman, *Phys. Rev. Lett.* **74**, 5144 (1995).

- ¹³A. J. Millis, Boris I. Shraiman, and R. Mueller, Phys. Rev. Lett. (to be published).
- ¹⁴J. Zaanen and P. B. Littlewood, Phys. Rev. B **50**, 7222 (1994).
- ¹⁵G. A. Thomas, D. H. Rapkine, S. A. Carter, A. J. Millis, T. F. Rosenbaum, P. Metcalf, and J. M. Honig, Phys. Rev. Lett. **73**, 1529 (1994).
- ¹⁶J. K. Freericks and M. Jarrell, Phys. Rev. Lett. **75**, 2570 (1995).
- ¹⁷See, e.g., T. Katsufuji, Y. Okimoto, and Y. Tokura, Phys. Rev. Lett. **75**, 3497 (1995), and references therein.
- ¹⁸J. Goodenough, Phys. Rev. **100**, 564 (1955).
- ¹⁹J. Kanamori, J. Appl. Phys. Suppl. **31**, 145 (1961); J. B. A. A. Ellemans, B. vanLaar, K. R. vanderVeer, and B. O. Loopstra, J. Solid State Chem. **3**, 238 (1971).
- ²⁰G. F. Koster, A. Dimmock, R. G. Wheeler, and H. Statz, *Representations of the 32 Point Groups* (MIT Press, Cambridge, MA, 1963).
- ²¹A. A. Abrikosov, L. P. Gorkov and I. E. Dzyaloshinski, *Methods of Quantum Field Theory in Statistical Physics* (Dover, New York, 1963).
- ²²N. Furukawa, J. Phys. Soc. Jpn. **63**, 3214 (1994).